Journal of Pharmaceutical Innovation (2024) 19:9
https://doi.org/10.1007/s12247-024-09815-z

ORIGINAL ARTICLE

Integrated Continuous Process Design for Crystallisation, Spherical Agglomeration, and Filtration of Lovastatin

Cameron J. Brown[1,2] · John McGinty[1,3] · Muhammad T. Islam[1,2] · Nazer Rajoub[1,2] · Omid Arjmandi-Tash[4] · Sara Ottoboni[1,3] · Muhid Shahid[1,3] · Stephanie J. Urwin[1] · Ye Seol Lee[5] · Magdalene W. S. Chong[1,6] · Foteini Papathanasiou[2] · Aruna S. Prakash[1,7] · Elke Prasad[1,2] · Bronwyn Spence[6] · Jan Sefcik[1,3] · John Robertson[1,2] · Rachel Smith[4] · James D. Litster[4] · Chris J. Price[1,3] · Alison Nordon[1,6] · Claire S. Adjiman[5] · Alastair J. Florence[1,2]

Accepted: 2 February 2024
© The Author(s) 2024

Abstract

Purpose This work seeks to improve the particle processability of needle-like lovastatin crystals and develop a small-footprint continuous MicroFactory for its production.

Methods General conditions for optimal spherical agglomeration of lovastatin crystals and subsequent product isolation are developed, first as batch processes, and then transferred to continuous MicroFactory operation.

Results Methyl isobutyl ketone is a suitable bridging liquid for the spherical agglomeration of lovastatin. Practical challenges including coupling unit operations and solvent systems; mismatched flow rates and inconsistent suspension solid loading were resolved. The successful continuous production of lovastatin spherical agglomerates (D_{50} = 336 µm) was achieved. Spherical agglomeration increased the density of the bulk lovastatin powder and improved product flowability from poor to good, whilst maintaining lovastatin tablet performance.

Conclusion A continuous, integrated MicroFactory for the crystallisation, spherical agglomeration, and filtration of lovastatin is presented with improved product particle processability. Up to 16,800 doses of lovastatin (60 mg) can be produced per day using a footprint of 23 m^2.

Keywords Continuous manufacturing · Process intensification · Pharmaceutical drug substance · Spherical agglomeration

✉ Alastair J. Florence
alastair.florence@strath.ac.uk

1 EPSRC Future Manufacturing Research Hub for Continuous Manufacturing and Advanced Crystallisation (CMAC), University of Strathclyde, Glasgow G1 1RD, UK

2 Strathclyde Institute of Pharmacy & Biomedical Science, University of Strathclyde, Glasgow G4 0RE, UK

3 Department of Chemical and Process Engineering, University of Strathclyde, Glasgow G1 1XJ, UK

4 Department of Chemical & Biological Engineering, University of Sheffield, Sheffield S1 4LZ, UK

5 Department of Chemical Engineering, Institute for Molecular Science and Engineering, Sargent Centre for Process Systems Engineering, Imperial College London, London SW7 2AZ, UK

6 WestCHEM, Department of Pure and Applied Chemistry and Centre for Process Analytics and Control Technology (CPACT), University of Strathclyde, 295 Cathedral Street, Glasgow G1 1XL, UK

7 National Physical Laboratory, Technology & Innovation Centre, 99 George Street, Glasgow G1 1, UK

Introduction

Continuous manufacturing has a significant role to play in the future supply of medicines. It provides significant opportunities to deliver sustainability, flexibility, and the required quality whilst also reducing the risks and costs associated with process development, scale-up, and technology transfer from development to commercial supply [1–3]. The impact of COVID-19 on global supply chains has further highlighted the need for supply security and to accelerate the adoption of technologies that can support rapid scale-up in the supply of safe, effective, and quality medicines in response to emergencies.

Several approaches to advance continuous processing have been demonstrated from the development of individual unit operations in drug substance (active pharmaceutical ingredient (API)/new chemical entity (NCE)) development [1, 4–6] through to continuous drug product (DP) manufacture [7]. In addition, complete end-to-end approaches have

Published online: 01 March 2024

been developed that combine API and DP manufacturing in a single integrated process chain, together with multiple innovations in process technologies, analytics, and control [8–13]. Although these examples go far beyond the norms of traditional batch pharmaceutical manufacturing, the opportunities, benefits, and suitability of continuous manufacturing to be implemented within existing quality and regulatory frameworks are evident from the growing number of marketing approvals secured to date [14].

Methods to support and inform the design of robust continuous pharmaceutical processes include development workflows aimed at reducing development [4, 6]; predictive design, modelling, and digital twins aimed at providing integrated modelling frameworks to simulate materials, processes, and products to enable the implementation of digital design approaches [15–19] as well as innovative continuous processing technologies [20–23]. Whilst the concept of MicroFactories has been initiated from discrete manufacturing settings [24], the application of the principles of small-footprint, flexible, modular, and continuous MicroFactories is of particular interest [25]. Such small footprint, highly automated, intensified, and reconfigurable equipment chains can potentially support the production of multiple products whilst also reducing the environmental impact [26]. MicroFactory or plug-and-play type equipment configurations have been developed for API [25, 27] and DP [28] applications, building a growing technology and evidence base to inform and advance future adoption.

The focus of this work is to develop a continuous MicroFactory-based process for lovastatin that enables an intensified process chain for particle engineering at the API-DP interface. The objective is to establish an integrated continuous crystallisation, spherical agglomeration, and isolation process for spherical agglomerates of lovastatin.

Lovastatin is a cholesterol-lowering drug that reduces the risk of cardiovascular disease. It is sparingly soluble in aqueous solution, but it has good solubility in a wide range of organic solvents. Of interest here is the preference to form needle-shaped crystals [29] (with aspect ratios in the range of ~ 1:1:100–1000, depending on the solvent). Given the challenging bulk and material properties often encountered with needle-shaped crystals, methods to modify and control particle properties are of considerable interest. Although undesirable morphologies can be modified using additives [30], we have also previously demonstrated a reduction in the aspect ratio by controlling the crystallisation of process conditions in the unseeded antisolvents of lovastatin in an acetone/water antisolvent system [31]. Using a high supersaturation and applying ultrasound during the solution/antisolvent mixing not only reduced the aspect ratio but also produced significant fouling and encrustation; conditions that reduced these unwanted phenomena gave the most needle-like lovastatin crystals. Spherical agglomeration presents an alternative particle engineering strategy that can convert poorly flowing primary needle crystals into spherical, well-flowing agglomerates [32–34]. Through careful selection and design of the formation processes, the size and mechanical properties can be achieved that allow streamlined development and operation of critical downstream processes such as feeding, blending, and compaction. The process involves the addition of a bridging liquid to bind primary particles together whilst suspended in the dispersing liquid phase. This presents a challenging design space for an integrated multistep continuous process involving antisolvent crystallisation, spherical agglomeration, and filtration, washing, and drying of agglomerates.

Here, we present the development of a batch spherical agglomeration process and its integration into a continuous MicroFactory for the crystallisation, spherical agglomeration, and filtration of lovastatin. A 300 µm agglomerate size was targeted to ensure uniformity with DP processing conventions. The direct transfer of batch conditions to continuous processing presented practical challenges with respect to vessel sizes and flow rates, which were addressed, and the benefits of using agglomerated particles were demonstrated in bulk density and compression studies.

Materials and Methods

Materials

Lovastatin (98.5–101.0% dried basis assay, total impurities ≤ 0.5%) was purchased from Molekula Ltd. Organic solvents acetone (≥ 99.8%), toluene (≥ 98%), heptane (≥ 99%), and methyl isobutyl ketone (MIBK) (> 99.0%) were purchased from VWR International Ltd. Deionised and filtered water was supplied by an in-house Millipore Milli-Q system. Avicel® PH-101 was obtained from FMC Biopolymer, Pharmatose® 50 M (α-lactose monohydrate) of the pharmaceutical grade was purchased from DFE and Alubra™ (sodium stearyl fumarate PG-100) of pharmaceutical grade from FMC Biopolymer.

Batch Process Methods

Spherical Agglomeration Bridging Liquid Screening

Following established guidelines for spherical agglomeration solvent choice [35], 13 bridging liquids (BL) were screened (Table 1). For each BL screened, 0.4 g lovastatin was suspended in 8 g water (1:20 mass ratio) in an 8-mL vial fitted with an overhead pitch-blade impeller. The vials were placed in the crystalline (Technobis) and stirred for 10 min at 2000 rpm. Aliquots (20 µL) of BL were added

Table 1 Solvents screened as bridging liquids for the spherical agglomeration of lovastatin in water

Solvent class	Solvents
Ethers	Tert-butyl-methyl ether
Acetates	Butyl acetate, ethyl acetate, isopropyl acetate, propyl acetate
Ketones	Methyl-isobutyl ketone (MIBK), methyl-ethyl ketone
Alkanes	Pentane, hexane, cyclohexane, heptane
Aromatics	Toluene, chlorobenzene

with a pipette, with 10 min of stirring in-between, until an agglomerate or paste was formed.

Batch Spherical Agglomeration

Lovastatin material equal to 10 wt% was suspended in a dispersing liquid solution of water/acetone in a 1000 mL OptiMax 1001 Thermostat (Mettler Toledo) equipped with a Hastelloy pitch-blade turbine impeller (45 mm in diameter). Temperature was kept constant at 20 °C and monitored via the built-in Pt100 temperature probe. The vessel was also equipped with focused beam reflectance measurement (FBRM, Mettler Toledo G400) and particle vision measurement (PVM, Mettler Toledo V819) probes. The slurry was stirred at 700 rpm for approximately 15 min to ensure complete suspension of primary crystals, followed by the addition of the bridging liquid at 100 µL/min (Dolomite Mitos P-Pump) until a bridging liquid to solid ratio (BSR, Eq. (1)) of 0.7 mL BL/g solid was achieved. V_{BL} is the volume of bridging liquid, and *mAPI* is the mass of lovastatin primary particles to be agglomerated.

$$BSR = \frac{V_{BL}}{m_{API}} \tag{1}$$

Batch Filtration, Washing, and Drying

Benchtop filtrations of slurries were performed in a modified Biotage VacMaster with a V850 vacuum controller (BÜCHI) [5]. The rack inside the filter chamber was modified to accommodate up to four 50-mL graduated cylinders; the valve assembly on the chamber lid comprised a pair of PTFE valves. Biotage ISOLUTE 70-mL single-fritted polypropylene reservoirs with 20 µm pore size were used to filter 50 mL of sample slurry and wash and deliquor the cake. The required level of vacuum inside the glass tank was confirmed on the vacuum controller, and the valve below the filter tube was opened to allow filtrate to flow through the medium into the graduated cylinder. Simultaneously, a stopwatch was started to time the filtrate flow; the time taken to accumulate 10, 20, 30, and 40 mL of filtrate was noted. On reaching dryland both PTFE valves were closed, the filter tube and the upper PTFE valve were removed, and the mass of the tube and filter cake was measured along with the filter cake thickness. The tube was then placed on the next valve on the top of the filter chamber in preparation for washing.

The required quantity of wash solvent was transferred to the top of the cake by slowly running the wash down the wall of the filter tube using a disposable pipette. Care was taken to minimise disturbance of the filter cake surface and mixing of the clean wash liquor with the mother liquors in the cake. Moving the filter tube to another position with an empty glass cylinder allowed deliquoring using the same vacuum set for the filtration and washing step. Deliquoring stopped when the bubble point was reached, and air freely passed the cake and filter media.

The cake was then dried using an in-house developed drying apparatus [36], utilising static drying at 60 °C with flowing hot nitrogen at 2 bar. A nitrogen flow rate of 0.3 L/min was selected for both drying setups. The temperature of the drying gas was controlled by flowing it through a coil of copper pipe maintained at 60 °C.

Continuous Process Methods

Continuous Anti-solvent Crystallisation Screening

Our previous study identified acetone/water as an appropriate solvent system for unseeded anti-solvent crystallisation of lovastatin [31], and the same equipment configuration was used here. A lovastatin solution at 0.0916 g/g (90% of the previously measured maximum solubility) in 90:10 w% acetone to water at 25 °C was pumped through a Y-piece to split the feed into two opposite ports of an X-mixer. Pure water as an antisolvent was fed into the centre channel. As process monitoring within the X-mixer is limited, the outlet of the X-mixer was fed into a 1-L stirred vessel equipped with FBRM (Mettler Toledo G400) and FTIR (ABB MB3000) probes. The output from the X-mixer was collected in the stirred vessel until the feedstocks were depleted.

Continuous Stirred Tank Crystallisation (CSTR)

To perform continuous crystallisations, a 2000-mL stirred tank vessel was used. Inlet flows of feed solution (lovastatin/water/acetone solution) and antisolvent (water) were controlled via gear pumps (Tuthill) with the flow rate, temperature, and density monitored by flow metres (Bronkhorst). Antisolvent was supplied at ambient temperature (22 °C), whereas the feed solution was supplied at 50 °C, and trace-heated transfer was used to maintain this temperature during transfer to the vessel. Discharge from the vessel was via a dip pipe with its end position at a liquid height equal to

a fluid volume of 1050 mL (whilst under agitation). Discharge was performed periodically under positive nitrogen pressure. This resulted in a maximum operating volume of 1200 mL with a 150 mL discharge of slurry over 13 s every 2.78 min. Vessel temperature was maintained at 25 °C using an external heater/chiller. For process monitoring, the vessel was also fitted with an FBRM probe (Mettler Toledo G400) through a side arm and a Fourier transform infrared (FTIR) probe through the lid. A schematic of the equipment is shown in Fig. 1.

The FTIR spectra were acquired using an MB3000 spectrometer (ABB) equipped with a 12 mm diamond attenuated total reflectance (ATR) probe. Spectra were acquired in absorbance mode using a resolution of 4 cm^{-1} and 8 scans, over the range of 2000 to 500 cm^{-1} and using a gain of 3600. The reference spectrum was acquired with the probe in air, and spectra were acquired every 30 s. Commencement of FTIR spectral acquisition coincided with the starting of acoustic emission (AE) monitoring (*ca.* 7 min after starting the pumps). Data analysis was performed in Matlab (version R2018a, Mathworks) using PLS_Toolbox (version 8.6.2, Eigenvector Research). The partial least squares (PLS) calibration model constructed for the prediction of acetone mass fraction (solvent composition) during the antisolvent crystallisation of lovastatin has been described elsewhere [31].

The broadband AE instrumentation comprised a Nano30 piezoelectric transducer (Physical Acoustics Limited), which was sensitive to frequencies up to 750 kHz, attached to a 2/4/6C (BY-SYS) preamplifier (Physical Acoustics Limited). The preamplifier required a 28-V power supply (Physical Acoustics Limited), and the gain of the preamplifier was set to 60 dB. The output of the preamplifier was connected to a 54642A oscilloscope (Agilent), which was linked to a laptop through a general-purpose interface board (GPIB) to a universal serial bus (USB) connection. The transducer was attached to the outside wall of the vessel; to ensure effective transmission between the piezoelectric transducer and the vessel, a layer of high vacuum grease (DowDuPont) was applied between the transducer and vessel wall glass, with the transducer secured in position using a double layer of electrical tape and a cable tie. AE signals were acquired using a sampling rate of 2 MHz with each signal comprising 4000 points. Signals were acquired every 2 s with a collection of data automated using a program written in the C programming language [37]. Data analysis was carried out in Matlab (version R2019a, Mathworks). The complex Fourier transform of each signal was calculated, and then the power spectrum of each signal was computed [38, 39]. The AE data acquired upon resuming FBRM data acquisition were discarded, giving 93 and 102 min of AE data for the crystallisation-only experiment (section "Continuous Crystallisation and Isolation") and crystallisation with spherical agglomeration experiment (section "Continuous Spherical Agglomeration and Isolation"), respectively. Representative spectra of the AE from the particles formed in the two experiments were calculated over a 21 min period (60 to 81 min for crystallisation-only

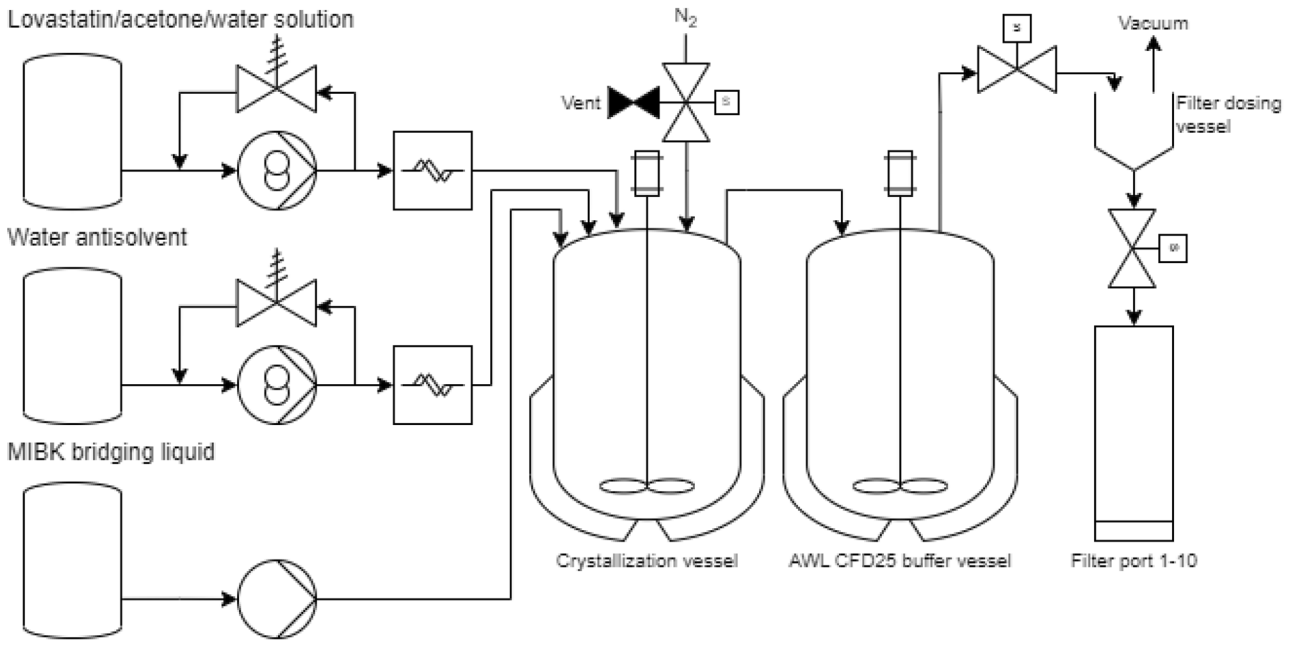

Fig. 1 Schematic of continuous crystallisation, spherical agglomeration, and filtration process equipment

experiment, and 75 to 96 min for crystallisation with spherical agglomeration experiment) during which the FBRM was paused. To normalise the spectra with respect to area, the total signal areas were calculated by summing the intensities of the signals over the entire frequency range [37, 39]. To improve the signal-to-noise ratio, 30 spectra were co-added to give a composite spectrum every 1 min. Principal component analysis (PCA) was performed using PLS_Toolbox (version 8.6.2, Eigenvector Research) on the mean-centred data across the entire frequency range.

For start-up, the vessel was partially charged with 250 g of a 5:95 w% acetone to water mixture before the feed solution and antisolvent pumps were turned on at a rate of 3.74 and 50.50 g/min, respectively. The stirrer speed was increased from 50 to 700 rpm over the course of solution addition until the operating volume was achieved. Process samples were collected from the outlet of the discharge every 30 min for off-line analysis; these were vacuum-filtered using a Büchner funnel, washed with water, and dried prior to analysis. Product material was collected and combined from the third residence time onward.

Continuous Spherical Agglomeration

Continuous spherical agglomeration was performed in the same manner as described for the continuous stirred tank crystallisation but with the addition of a further inlet for MIBK as bridging liquid addition. In this case, whilst the feed solution and antisolvent pumps were engaged, a third pump (Dolomite Mitos P-Pump) was used to deliver bridging liquid at a rate of 0.850 g/min. All other experimental conditions remained the same.

For both the continuous crystallisation (section "Continuous Stirred Tank Crystallisation (CSTR)") and spherical agglomeration a minimum run time of 7 to 10 residence times was targeted to achieve and demonstrate steady-state operation [40, 41]. Both processes were successfully run five times over a series of campaigns to demonstrate process robustness. The results presented here are from a single campaign where the product was material characterised and used downstream in tabletting.

Continuous Filtration, Washing, and Drying

Continuous isolation of product slurries from both the continuous crystallisations (section "Batch Spherical Agglomeration") and continuous spherical agglomeration (section "Continuous Filtration, Washing, and Drying") was achieved using an AWL CFD25 continuous filtration, washing, and drying system, which has ten operational ports. The implemented operating mode is summarised in Table 2 (and Fig. S1). To avoid filter blinding during operation a cleaning-in-place process with acetone was performed every five indexes in ports 1, 2, 3, and 4.

As the level of dryness achievable in the AWL CFD25 is limited due to the cycle times. Further drying of the product powder was conducted in a vacuum oven until a minimum loss of drying of 0.5%, in line with ICH guidelines for residual solvents [42].

Product Characterisation and Tabletting

Scanning Electron Microscopy (SEM)

Solid, dry samples of lovastatin spherical agglomerates were attached to the aluminium stubs with carbon tape. Prior to the analysis samples were coated with a 10-nm gold layer using EM ACE 200 sputter-coater (Leica Inc.). SEM images were recorded in backscattered mode at 1000 V using Field Emission Scanning Electron Microscope (Keysight) at magnifications 500 × and 2000 × from three distinct positions.

Particle Size Distribution (PSD) Measurements

Off-line laser diffraction measurements were conducted using the Mastersizer 3000 (Malvern Instruments Limited) fitted with a Hydro Insight (i.e. flow microscopy, Malvern Instruments Limited high-resolution digital camera attachment. For dry solid samples, a few drops of water were added to the powder to form a paste, and for process

Table 2 Summaryof AWL CFD25 method

Operation	Method	Ports used
Transfer from feed slurry tank	6 × 60 mL aliquots, 20-s filtration time	1
Washing and deliquoring	4 equivalent cake volumes each, 30 s each wash followed by deliquoring Wash 1: water; wash 2: n-heptane; wash 3: n-heptane	2–4
Drying station	1 min at 40 °C, 2 bar N_2 at 0.3 L/min	5–9
Ejection of the cake		10

samples, the slurry was used without modification. The sample was dispersed in the Hydro MV cell (Malvern Instruments Limited, UK) by gradually adding the paste to the cell to reach a laser obscuration between 5 and 20%, although typical obscuration was around 6–8%. The dispersed sample was stirred at 2000 rpm, and each measurement was taken for 10 s (including background). Five 10-s measurements were taken and then averaged for each sample. Measurements were made without ultrasound. The unit was cleaned with acetone in between samples. Laser diffraction measurements are expressed as the volume-weighted distribution of equivalent sphere diameter.

Isolated product samples were analysed using the Morphologi G3 (Malvern Instruments Limited, UK) to obtain the particle size and aspect ratio distributions. The procedure involved placing 7 mm^3 of solid sample into the integrated powder dispersion unit and, unless otherwise stated, using a low energy dispersion method (1 bar) to form a circle of flat separate particles on the glass plate. The instrument then scanned the powder sample whilst capturing images with the use of 5 × magnification. For all the particles captured, the full range of size and shape properties were determined by the integrated image analysis software (Malvern Morphology v.8.12). Image filters were applied to the raw data to remove artefacts such as dust and fibres. The particle size results were reported as volume-weighted circle equivalent (CE) diameter with CE10, CE50, and CE90. The span of a PSD for all measurement methods was calculated using Eq. (2). In general, smaller values for span are preferred.

$$Span = \frac{D_{90} - D_{10}}{D_{50}} \quad (2)$$

Time-of-Flight Secondary Ion Mass Spectrometry (ToF–SIMS)

For each sample, double-sided adhesive carbon tape was attached to a small piece (~ 1 cm^2) of silicon wafer, and a small amount of the sample was added to the exposed adhesive side. Any excess/loose particulates were removed from the tape using a gentle stream of nitrogen before the sample was placed into a sample holder and inserted into the ToF–SIMS.

Analyses were carried out on a TOF.SIMS 5 mass spectrometer (IONTOF GmbH, Germany). A 30-keV Bi_3^+ primary ion beam was used for analysis, and an electron flood gun was used for charge compensation. The surface potential of the sample holder was optimised for each analysis. All samples were analysed in positive and negative ionisation, and in two different modes; (1) low-resolution spectrometry mode employing higher primary ion beam currents for better ion intensity, and (2) delayed extraction mode for enhanced spatial resolution and mass resolving power. The data shown here has been acquired in positive ionisation with delayed extraction using a primary ion beam current of 0.06 pA at a cycle time of 120 µs and with a 55-ns extraction delay. Data was acquired over a 500 × 500 µm target area, a pixel count of 512 × 512 pixels, and a primary ion dose density of 1.04×10^{11} ions/cm^2. Samples were analysed and processed using SurfaceLab v7.0 software (IONTOF GmbH, Germany).

Bulk and Tapped Density

Measurements were performed according to the British Pharmacopoeia method [43]. For the bulk density, approximately 100 g of the test sample weighed with 0.1% accuracy was poured through a funnel into a dry graduated cylinder of 250 mL with 2 mL grading divisions. The cylinder was inverted once before the unsettled apparent volume (bulk volume) (V_0) was read so that disturbances of the powder bed were minimised. For tapped density (Dual Autotap, Quantachrome), the graduated cylinder with the sample powder (obtained from the bulk density measurements) was mechanically tapped 10, 50, and 1250 times, and the corresponding volumes V_{10}, V_{500}, and V_{1250} were read. When the difference between V_{500} and V_{1250} was larger than or equal to 2 mL, another 1250 taps were conducted.

Direct Compression

Tablets were produced by a single punch tablet press (Korsch XP1, Korsch AG) at 20 tablets per min, on which 9 mm diameter, round, and flat-faced punches were installed. The tablet press was operated in the automatic, single-stroke mode to allow for upper punch compression force (UPCF), lower punch compression force (LPCF), ejection force (EF), upper punch displacement (UPD), and lower punch displacement (LPD) to be recorded. The upper punch was being adjusted to several positions such that upper punch compression forces in the range of 0.5 to 20 kN were obtained. Ten replicate measurements were taken for each of the UPD to allow for statistical processing and interpretation of the results.

In total four formulations, with a target mass of 200 mg, were tabletted: pure crystallised lovastatin, pure spherical agglomerate lovastatin, 70:20:10 Pharmatose to Avicel to crystallised lovastatin and 70:20:10 Pharmatose to Avicel to spherical agglomerated lovastatin. For the pure crystallised lovastatin, external lubrication and manual filling of the die were necessary.

Tablet mass was measured on a Quintix124-1S (Sartorius) balance. Tablet thickness and diameter were measured on the Absolute digimatic indicator 1D-C1012XB (Mitutoyo), and tablet hardness on tablet hardness tester HC6.2 (Kraemer Electronik). Tablet solid fraction was calculated from the measured tablet dimensions and mass.

Results

Conversions of Batch Crystallisation to Continuous Conditions

In our previous study of unseeded antisolvent crystallisation of lovastatin from acetone/water, it was possible to generate lovastatin crystals with a range of particle sizes and aspect ratios [31]. The solution to antisolvent ratio was found to be the dominant process parameter in controlling size and aspect ratio; however, the 3:1 ratio used in previous work produced crystals that were too large to achieve the target final particle size of 300 µm as some of the crystals produced already exceed this size and the system showed rapid depletion of supersaturation in only 3.5 min. The initial configuration to convert the fed-batch process to a fully continuous process used a 1:1 solution-to-antisolvent ratio, with the solution prepared at 90% of the maximum solubility at 90:10 w% acetone to water resulting in a final composition of 45:55 and a minimum residence time (τ) of 5 min to ensure depletion of supersaturation.

Batch Spherical Agglomeration

When screening a BL for spherical agglomeration behaviour, three distinct outcomes are observed. When the added BL is either not feasible or is present in insufficient quantity to initiate agglomeration, primary particles remain suspended in the solution (Fig. 2a). Once enough of a suitable BL has been added, spherical agglomerates form (Fig. 2b), with distinctly spherical shapes in ideal conditions. Where excess BL is added, a paste will form (Fig. 2c). Overall Fig. 2a–c demonstrates the impact of the BSR ratio on the spherical agglomeration process outcomes. Of the thirteen solvents screened for lovastatin (Table 1), only toluene (BSR = 0.21), n-heptane (BSR = 1.00), and MIBK (BSR = 1.76) exhibited the formation of spherical agglomerates, consistent with the literature [44].

The three candidate BLs were taken forward to preliminary integrated batch spherical agglomeration experiments. In each, lovastatin crystals were dispersed in 45:55 w% acetone to water, a solvent mixture consistent with the post-crystallisation mother liquid composition, and the candidate BL was added. Due to low interfacial tension between toluene and the acetone/water mixture, the initial droplets formed by the dolomite fluidic system quickly dispersed into finer droplets when mixing in the vessel. As these droplets were much smaller than the lovastatin crystals, agglomeration proceeded via a distribution mechanism [33], and SEM images confirm the resulting loosely bound agglomerates (Fig. 2e). Low miscibility and high interfacial tension between n-heptane and 45:55 w% acetone to water created stable n-heptane droplets. Whilst spherical agglomerates

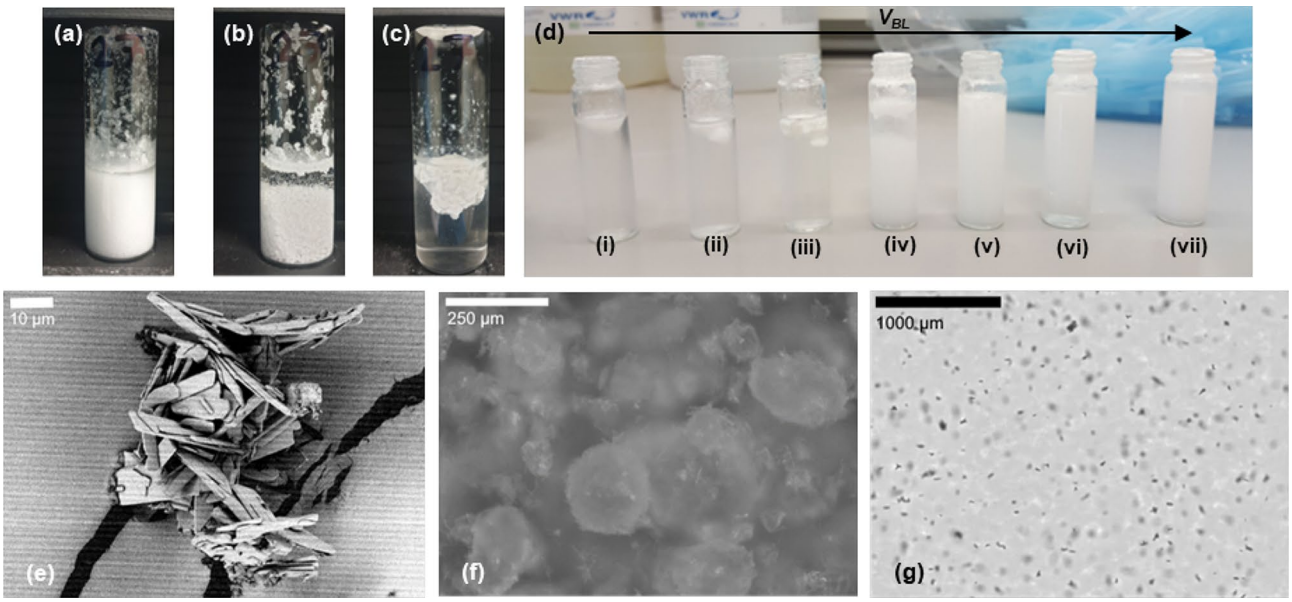

Fig. 2 Top: Results of BL screening. Differing stages of agglomerate formation from **a** no agglomerate formed due to wrong/insufficient bridging liquid, **b** agglomerate formation from correct BSR, **c** paste product due to excessive bridging liquid addition. **d** Effect of acetone concentration on MIBK as bridging liquid: (i) 0 wt% acetone, BSR = 0.30; (ii) 5 wt% acetone, BSR = 0.36; (iii) 9 wt% acetone, BSR = 0.40; (iv) 15 wt% acetone, BSR = 1.00; (v) 20 wt% acetone, BSR = 1.20; (vi) 25 wt% acetone, BSR = 1.40 and (vii) 30 wt% acetone, BSR = 1.60. Bottom: Results of batch spherical agglomeration trials **e** SEM image of loose agglomerate; BL, toluene. **f** In situ video microscopy image of agglomerates formed where BL, n-heptane, and **g** flow microscopy image of those agglomerates after isolation

were subsequently observed using PVM (Fig. 2f), upon isolation, these agglomerates had de-aggregated into their primary particles (Fig. 2g). These weak, loosely bound agglomerates observed when using toluene or n-heptane as a BL are due to the negligible solubility of lovastatin in these solvents, resulting in a lack of any driving force for the formation of crystalline bridges between primary particles that otherwise are required to impart structural integrity to the agglomerates.

The formation of lovastatin spherical agglomerates using MIBK as a bridging liquid has been reported previously where water was the dispersing liquid [44]. However, in this work adding MIBK to a suspension of lovastatin in 45:55 w% acetone to water produced no spherical agglomeration. The acetone/water/MIBK ternary solvent system has a large region of miscibility [45], and the added droplets of MIBK can therefore disperse creating a single solvent phase. This lack of phase-separated droplets means MIBK cannot act as a binder to initiate lovastatin spherical agglomeration under these conditions.

To investigate operation outside of the acetone/water/MIBK miscible region, a series of screening experiments was conducted where simultaneously increasing aliquots of acetone (5 to 30 wt%) and MIBK (resulting BSR 0.3 to 1.6) were added to a suspension of lovastatin in water (Fig. 2d, Table S1). This demonstrated that above 9 wt% acetone and a BSR of 0.4, spherical agglomerates did not form. Investigating further, when MIBK was added to a dispersion of lovastatin in 5:95 w% acetone to water, spherical agglomeration was successful, and the particle size distribution of the isolated agglomerates (Fig. 3a) showed a significant increase in size (D_{50} = 256 µm) compared to the primary particles (D_{50} = 29.2 µm), with the bimodal shape indicating some primary particles remain. As the size measurements and microscopy images were taken post-isolation, this demonstrates that under these conditions, the resultant agglomerates are strong enough to withstand isolation operations. Therefore, for an initial configuration to convert this process to a fully continuous process, it would operate with a dispersing liquid of 5:95 w% acetone to water, MIBK as a bridging liquid, and a 10 wt% solid suspension density of primary particles.

Batch Filtration and Washing

Using the spherical agglomerates formed in the batch trials, four filtration experiments were performed to identify the optimal filtration driving force to achieve effective filtration whilst preventing any agglomerate breakage, with screening of vacuum pressures up to 700 mbar (Fig. 3d). The appearance of a shoulder on the distributions when pressures higher than 63 mbar were applied indicates the limit of agglomerate mechanical resistance was reached and partial particle breakage occurred. Therefore, the applied pressure selected for all further filtration experiments (batch and continuous) was capped at 63 mbar. Further filtration experiments on slurries with solid densities of 1 w% or 10 w% demonstrated that the filtration of a lower suspension density produces a thin cake with rapid filtration times (Table S2), although the accuracy of the cake resistance values determined could be influenced by inadequate cake formation. It was concluded that a higher-density slurry would be preferred.

In the spherical agglomeration of lovastatin described (section "Batch Spherical Agglomeration"), the resultant mixture comprised the crystallisation solvent (acetone and water), antisolvent (water), and bridging liquid (MIBK). As lovastatin is soluble in acetone and MIBK, the presence of these solvents after washing can promote particle–particle cementation during drying leading to an increase in the size of particles or the formation of an unwanted solid cake after drying. Therefore, a washing strategy was designed to maximise mother liquor removal. A three-stage washing strategy was considered to maximise washing efficiency; an initial water wash to adequately rewet the deliquored cake from the filtration stage whilst removing residual acetone and MIBK, followed by two washes with n-heptane to remove water. As the solubility of lovastatin in water is negligible, dissolution of lovastatin during this process is not of concern. Washing with water promotes the removal of acetone and MIBK through displacement and diffusion and dilution in particle–particle pores. Using n-heptane for the final washing step replaces water with a solvent of much lower enthalpy of vaporisation and heat capacity so a lower drying temperature can be used, reducing energy requirements and drying times.

The effect of using two and four equivalent cake volumes (ECVs) for each washing stage on particle agglomeration and drying time was investigated (Table 3). Using two cake volumes (wash strategy 1) led to a reduced cake moisture content after 3600 s of drying when compared with four cake volumes. The wash solvent volume did not impact the particle size distribution.

Combining the results of the filtration, washing, and drying experiments, an initial configuration to convert this process to a fully continuous process is using a 10 wt% solid suspension density of spherical agglomerates, a filtration driving force of 63 mbar, washed once with water, then twice with n-heptane, each using two ECVs.

Process Integration

With each unit operation developed, the proposed continuous operation conditions can be coupled together to deliver a working concept of an integrated continuous process, as described by the process information summary map in Fig. 4. However, due to the semi-independent development of each unit operation, several discontinuities exist when attempting to couple the processes:

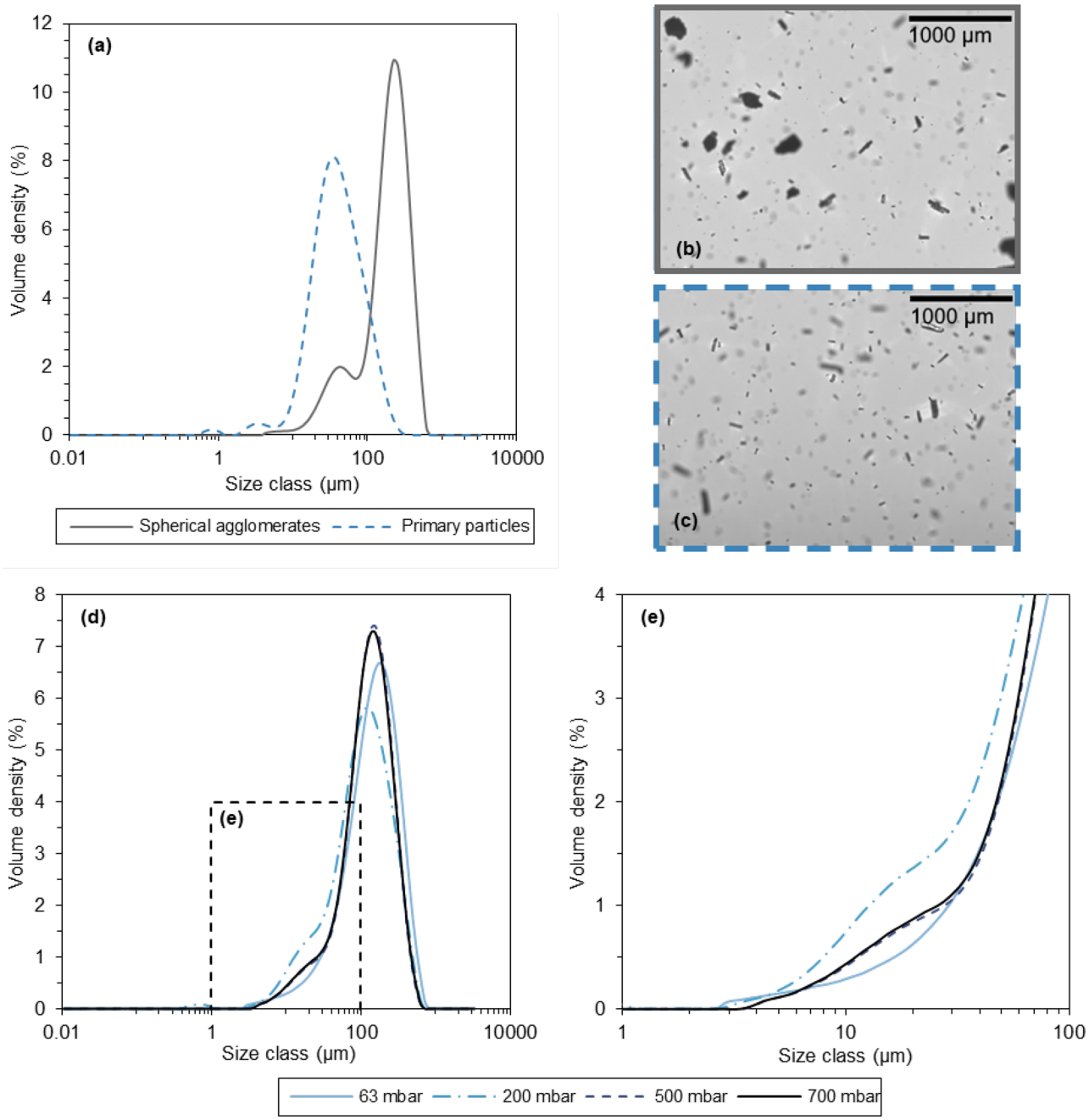

Fig. 3 Top: Results of batch spherical agglomeration trials using MIBK as bridging liquid in 5:95 w% acetone to water dispersing liquid. **a** Laser diffraction measurements of primary particles and resultant spherical agglomerate product. Flow microscopy images of **b** spherical agglomerates and **c** primary particles. Bottom: Results of filtration driving force study over **d** full measurement range and **e** narrower size range highlighting differences in fraction of small particles

1. The crystallisation operates with an end point consisting of 45:55 w% acetone to water. In contrast, it was demonstrated that for using MIBK as a bridging liquid, a 5:95 w% acetone to water ratio was required to ensure the formation of an immiscible phase (i.e. the values in Fig. 4a and b are not consistent).
2. To ensure rapid mixing in the crystallisation X-mixer, a high flow rate of solutions is required (385.24 g/min in total). To achieve the required residence time for the spherical agglomeration at this flow rate, a cascade of stirred tanks of a total volume of 27 L would be required (Fig. 4c). This is greater than could be accommodated

Table 3 Outcome of washing strategy and drying experiments

	Wash strategy 1	Wash strategy 2
Wash 1 (water) cake volumes	2	4
Wash 2 (n-heptane) cake volumes	2	4
Wash 3 (n-heptane) cake volumes	2	4
Particle size, D_{10} (μm)	42.6	41.3
Particle size, D_{50} (μm)	154	159
Particle size, D_{90} (μm)	362	351
Cake moisture after 180-s drying (%)	59.4	55.8
Cake moisture after 3600-s drying (%)	19.0	41.9

on the laboratory scale test bed. This total flow rate also exceeds the accessible throughput for filtration, washing, and drying cycles within the AWL CFD25 unit (Fig. 4d).

3. The slurry output from the crystallisation has a suspension density of 4.25 wt%. However, both the spherical agglomeration and filtration were developed to operate with a higher suspension density of 10 wt%. For filtration, this lower suspension density may lead to the formation of thinner cakes and poorer washing efficiency.

Several changes were implemented to address these discontinuities to fully integrate the process unit operations. The total throughput of the process was decreased to accommodate the AWL CFD25 constraints; the total flow rate into crystalliser was reduced from 385.25 to 54.25 g/min. Consequently, rapid mixing of solvent streams was no longer achievable, making the use of the X-mixer unfeasible, and the crystallisation equipment was changed to a continuous stirred tank configuration where mixing is controlled via the impeller speed, whilst not affecting the addition of antisolvent or BL. To produce a solution composition from the crystallisation compatible with the later addition of MIBK for the continuous spherical agglomeration, excess water was added during the crystallisation to reach an end point of 5:95 w% acetone to water. Despite this extra addition of antisolvent, this does not increase the lovastatin crystallised yield, as solubility is negligible beyond a 45:55 w% acetone to water solvent composition. One downside of this additional dilution is the production of a slurry with a lower suspension density impacting filtration efficiency (i.e. requiring multiple aliquots of slurry into the AWL CFD25 to produce sufficient filter cake). To mitigate this, a higher initial concentration of lovastatin was used by starting with a solution at an elevated temperature of 50 °C. As a result, the lovastatin feed concentration was increased from 0.0430 g/g solution to 0.1784 g/g solution. The resulting suspension has a slurry density of 1.2 wt% which was within the operable range for the filtration platform. The outcome of this is twofold; firstly, to overcome this dilute suspension (< 10 wt%), the operating protocol for the AWL CFD25 was modified (Table 2) to allow for multiple doses of slurry to be charged, creating a filter cake of

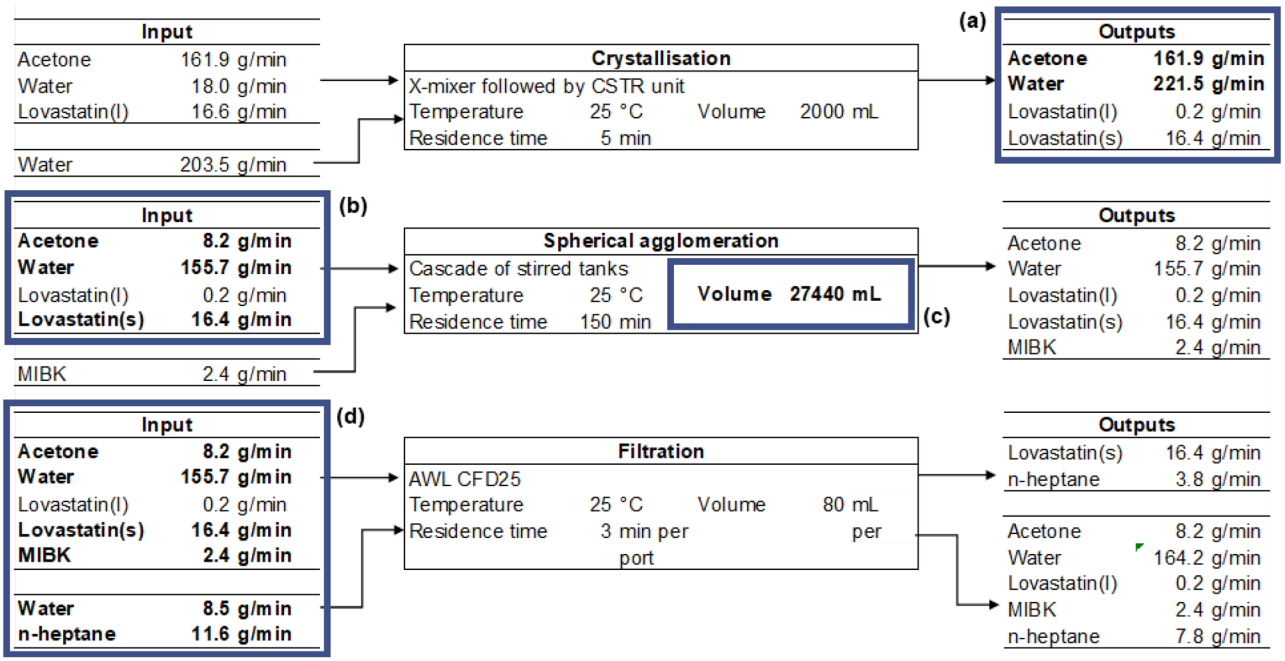

Fig. 4 Process information summary map for crystallisation, spherical agglomeration, and filtration unit operations based on independent development, with discontinuities between unit operations highlighted

the required minimum thickness. Secondly, the quantity of MIBK needed to be adjusted from previous experiments. To evaluate this, several continuous spherical agglomeration processes (section "Batch Filtration, Washing, and Drying") were carried out with different flow rates of MIBK, leading to different BSRs. The solution composition of these experiments relative to the two-phase boundary in the ternary system of acetone/water/MIBK is shown in Fig. 5a. It should be noted that the data used to define this phase boundary [45] is only for the ternary mixture of acetone/water/MIBK and therefore excludes the effect of lovastatin solute. Hence, this boundary was used as a guide only. When keeping the BSR constant to the batch (BSR = 0.4, Fig. 5a, orange square), the resulting solution (Fig. 5a, green diamond) is far from the two-phase boundary, and it was observed that spherical agglomeration did not occur. At the other extreme of increasing the MIBK flow rate to result in a composition within the two-phase boundary (Fig. 5a, yellow triangle), agglomeration was excessive and led to the formation of a paste adhering to the stirrer and vessel wall (Fig. 5b). Based on these results, the MIBK flow rate was chosen at 0.8 g/min to achieve a solution composition matching that of the batch spherical agglomeration (Fig. 5a, grey circle).

These trials also demonstrated that the residence time for continuous spherical agglomeration could be much shorter than the batch time. In the batch spherical agglomeration, BL (MIBK) addition was added at a controlled rate until a target BSR was reached. This addition time dictated the batch time. However, in the continuous spherical agglomeration experiments, the MIBK flow rate was required to be proportional to the acetone/water solution flow rate to maintain the desired composition. As a result, the continuous spherical agglomeration experiments only required sufficient residence time to allow for wetting and consolidation of the spherical agglomerates.

With all these changes considered, the new process is summarised in Fig. 6. Furthermore, with the crystallisation and spherical agglomeration able to occur over similar timescales, it was decided to intensify the process by simultaneously adding the feed solution (acetone/water/lovastatin), antisolvent (water), and bridging liquid (MIBK) together into a single continuous stirred tank, resulting in the method described in sections "Continuous Stirred Tank Crystallisation (CSTR)" and "Continuous Spherical Agglomeration".

Continuous Crystallisation and Isolation

In the following sections ("Continuous Crystallisation and Isolation" and "Continuous Spherical Agglomeration and Isolation"), both processes were successfully run four times over a series of campaigns to demonstrate process robustness and reproducibility. The results presented here are from a single campaign where the product was material characterised and used downstream in tabletting.

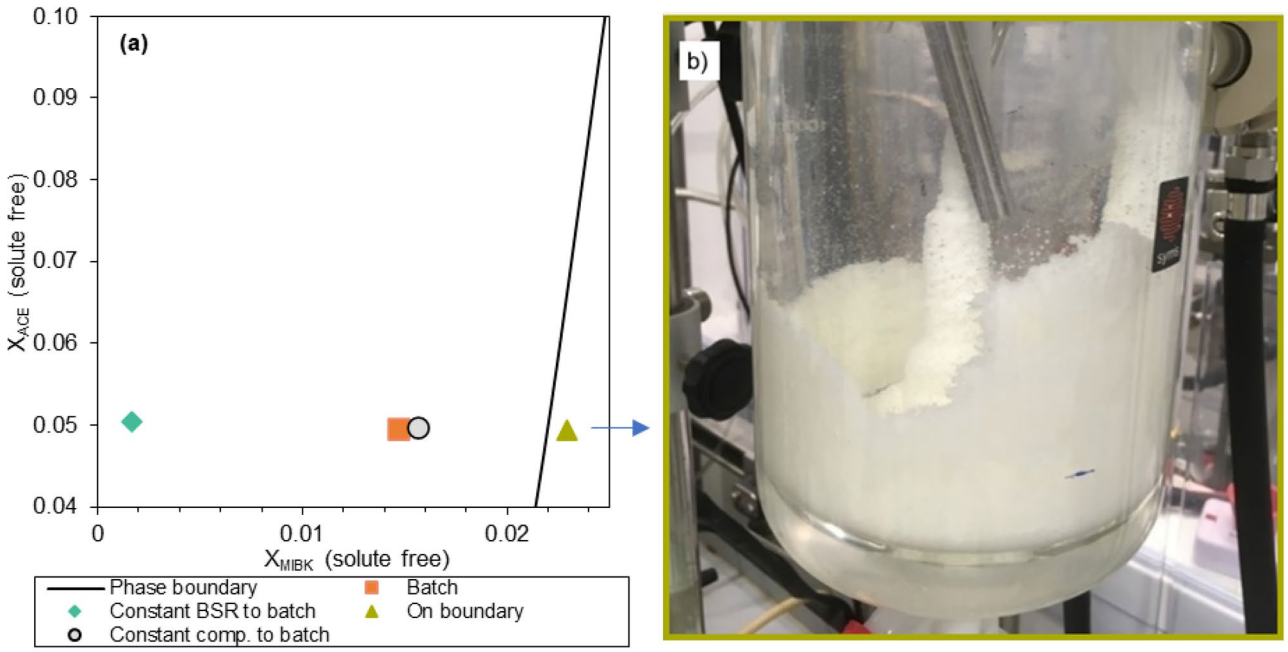

Fig. 5 **a** Solution solvent composition of experiments compared to the ternary acetone/water/MIBK system two-phase boundary [45] as a guide. **b** Paste-like agglomerates adhering to the stirrer and vessel wall formed with solution composition at the yellow triangle in **a**

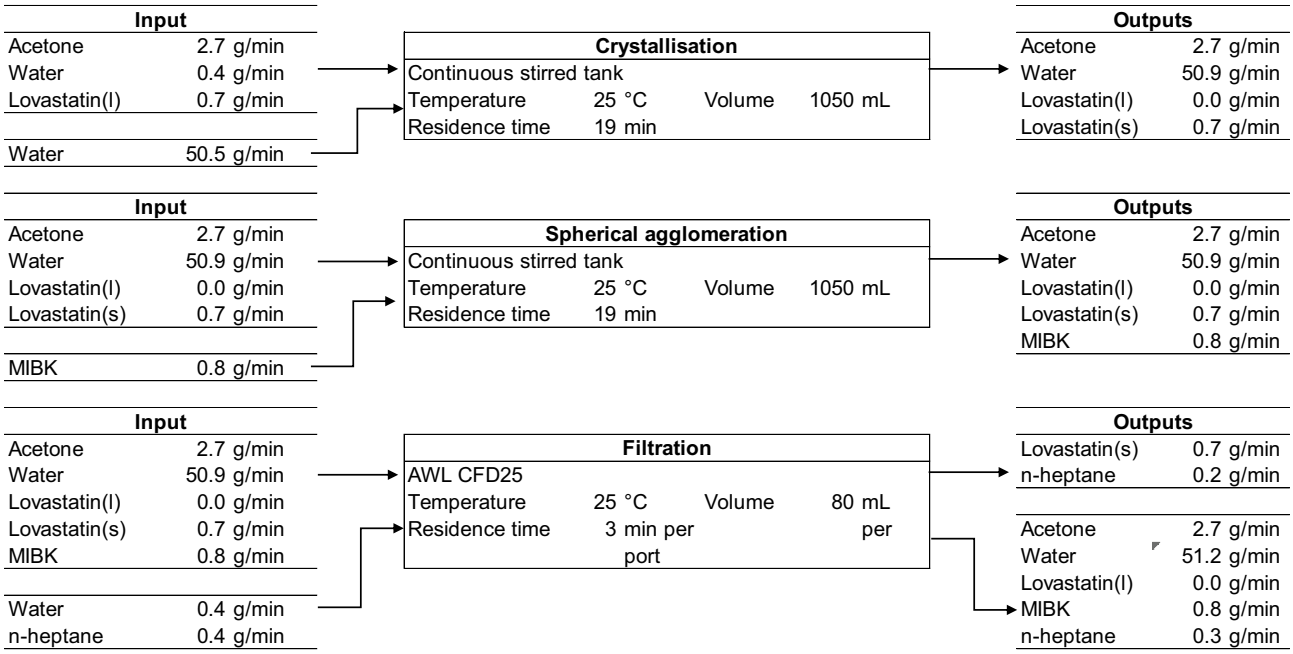

Fig. 6 Process information summary map for crystallisation, spherical agglomeration, and filtration unit operations after the redesign to produce an integrated process. Note: Crystallisation and spherical agglomeration are shown as separate process for clarity; however, in practice, they will occur simultaneously

The first unit operation in the process information map (Fig. 6), a continuous crystallisation experiment of lovastatin from acetone/water, was initially undertaken without continuous spherical agglomeration to validate the new proposed conditions. The process was monitored using FBRM and FTIR within the CSTR. Owing to the extensive fouling encountered in development work [31], in situ monitoring of solute concentration via UV–vis spectrometry was not used in these experiments. During process operation, FBRM data collection was paused for 38 min to allow for AE signals to be measured without noise interference. The crystallisation product was continuously isolated during process operation by filtration, washing with n-heptane (2 × 2 ECV), and vacuum drying. A mean predicted acetone fraction of 5.6 w% (standard deviation, $\sigma = 0.2$) in the solvent mixture corresponding to the expected value from the process information summary map was recorded for the first six FTIR spectra (corresponding to *ca.* 3 min); however, subsequently, this value begins to deviate (Fig. S3). Emergence of fouling was observed within the first 20 spectra collected (evidenced by lovastatin peaks in the FTIR spectra, Fig. S4), with fouling on the vessel walls also visually evident. In this instance, fouling has significantly hindered in situ spectroscopic monitoring.

Once the process began, the FBRM trends plateaued within two residence times ($\tau = 19$ min, Fig. S5), indicating a steady state had been achieved. Overall, the process ran without significant intervention for 3.5 h. Samples were taken from the process vessel every 30 min during operation (seven samples total), and the particle size distribution of the particles in these slurries was estimated using laser diffraction (Fig. 7a). A wide variation (range 281–912 µm) in the estimated D_{90} values was observed across the sampling range, for reasons that remain unclear, and Sample 3 was designated an outlier and was omitted from statistical analysis. The D_{10} and D_{50} values do not vary significantly across the six samples, with respective mean values of 43.7 µm ($\sigma = 15.9$) and 139 µm ($\sigma = 21.0$), indicating that the process had reached steady state within the expected two residence times. The span of the estimated particle size distributions was large, at 2.51. An increase in the FBRM fouling index was also observed at 145 min from 4 to 8.5%, at which point the probe was removed for cleaning before re-inserting (appears as a spike in counts, Fig. S5). Images of the sample suspension taken during particle size estimation (Fig. S6) confirm the presence of individual, unagglomerated crystals in the suspension.

The measured PSD (Fig. 7c). of the isolated lovastatin crystals are consistent with the process sample estimations (Tables S4 and S5), confirming that the isolation procedures did not induce any particle modification or agglomeration. The particle size D_{50} of the isolated product was measured at 135 µm, significantly larger than the seed material ($D_{50} = 38.5$ µm, Fig. S2 and Table S3).

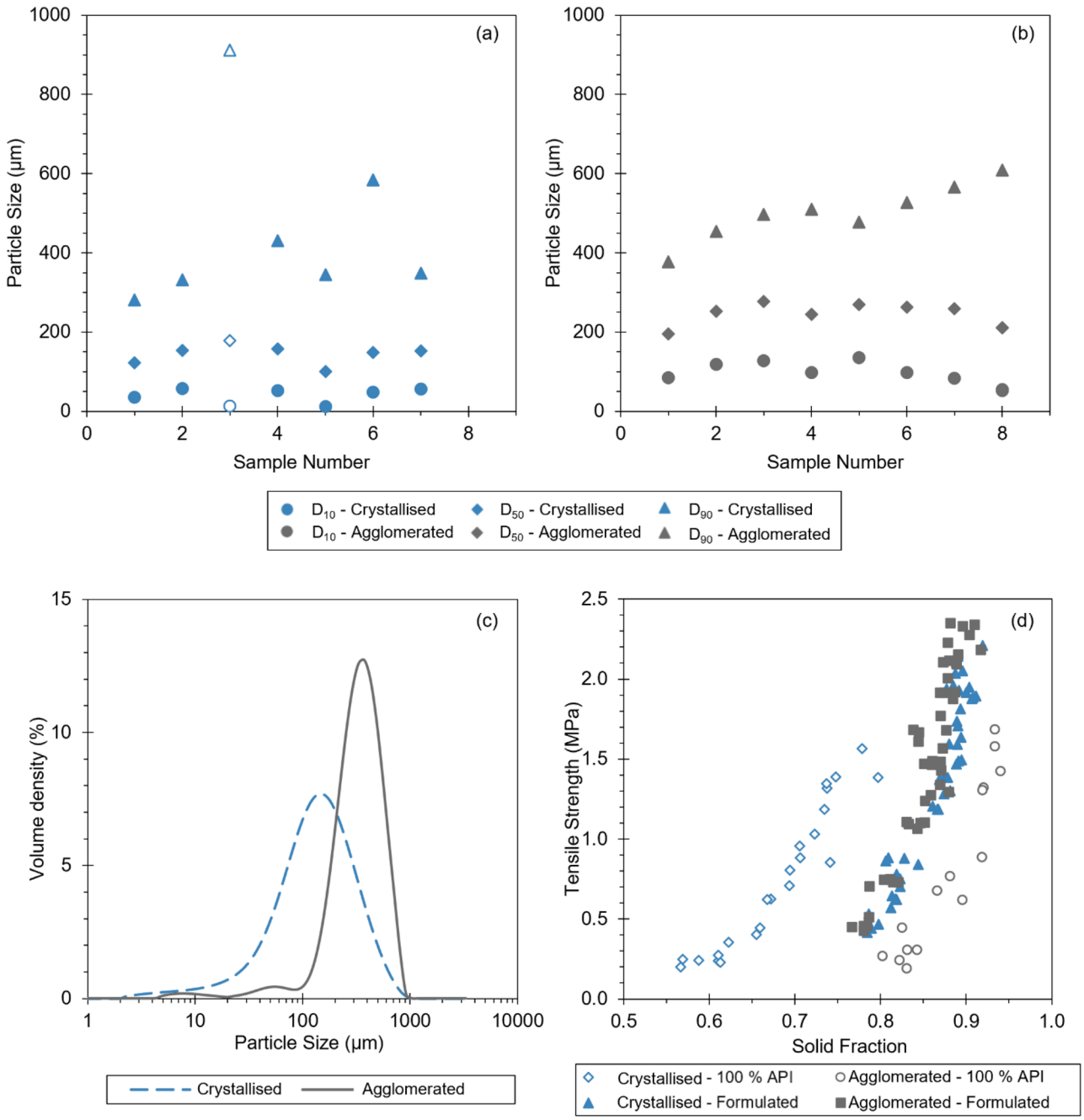

Fig. 7 **a** Estimated PSD metrics of process samples from continuous crystallisation experiment, sample 3 is designated as an outlier. **b** Estimated PSD metrics of process samples from integrated continuous crystallisation and spherical agglomeration experiment. **c** Particle size distribution of isolated product from the continuous crystallisation and integrated continuous crystallisation and spherical agglomeration experiments, showing the increase in particle size through agglomeration. **d** Comparison of compactability of tablets produced from crystallised and spherical agglomerated particles. Formulated tablet composition was 70:20:10 w% Pharmatose to Avicel to lovastatin particles. Each point is the average of ten replicates

Continuous Spherical Agglomeration and Isolation

Following the successful demonstration of the continuous antisolvent crystallisation and isolation of lovastatin, the operation of the fully integrated continuous crystallisation, spherical agglomeration, and isolation of lovastatin Micro-Factory was undertaken. The platform setup was identical to the previous continuous crystallisation operation (section "Continuous Crystallisation and Isolation"), with an added MIBK inlet to add BL, initiating the continuous spherical

agglomeration process and operating with a BSR value at a steady state of 1.43 mL/g (Fig. 6). FBRM monitoring of the process was paused for 35 min during the process to allow for AE measurements to be recorded without sound interference from the FBRM probe, like the continuous crystallisation experiment (section "Continuous Crystallisation and Isolation"). The process was successfully operated for 4 h; however, like the previous crystallisation experiment, significant fouling on the FTIR probe led to this data not being informative. Fouling of the ATR crystal was encountered even sooner (Fig. S3), and significant fouling was once again evident in the spectra as peaks attributed to lovastatin (Fig. S4).

Once the process began, the total FBRM counts rose rapidly (Fig. S7), reaching a maximum after 45 min, consistent with the crystallisation process reaching equilibrium. The total FBRM counts subsequently decreased, indicating a fewer total number of particles were present. A synchronous decreasing trend in counts with a chord length of 10–50 µm and an increasing trend in counts with a chord length of 50–150 µm suggest spherical agglomeration was taking place in the vessel. Like the FTIR probe, the FBRM probe showed significantly higher levels of fouling in comparison to the crystallisation-only process (fouling index range from 50 to 70% compared to 4%), leading to erratic trends from 120 min onwards. Therefore, these results are given for completeness but were not relied upon for subsequent analysis.

Comparison of representative AE spectra acquired of the particles formed in the two MicroFactory experiments indicates a larger overall amplitude (Fig. S8a) and an increase in the relative intensity of the signals at lower emission frequency (Fig. S8b-c) when spherical agglomeration is taking place, indicative of larger particles forming. PCA was carried out on the AE spectra from both experiments [39]. The loadings show principal component (PC) 1 is correlated with the spectrum across the entire frequency range. PC 2 is correlated and anticorrelated to signals below and above 14.5 kHz, respectively (Fig. S9). In the scores plot of PC 1 (35.4% variance) vs PC 2 (16.6% variance), the initial data from both experiments are in the same region (Fig. S10), which is expected as the vessel contents and conditions are comparable. As AE monitoring commences *ca.* 7 min into both experiments, with stirring gradually increased from 50 to 700 rpm as the vessel is filled, the vessel is not filled until *ca.* 10 min into AE monitoring. This is observed by the data from the first 10 min of both experiments located at mean PC 1 and PC 2 scores of − 5.6 and 0.4, respectively. As both experiments progress, the PC1 score increases, which is consistent with an increase in the amplitude of AE; this could arise from an increase in the size and/or number of particles [39]. However, the spectra acquired during crystallisation-only operation have negative PC 2 scores, whilst the spectra acquired during crystallisation with continuous spherical agglomeration operation have positive PC 2 scores (Fig. S10). This implies that more AE occurs at lower frequencies during crystallisation with continuous spherical agglomeration operation than with crystallisation only, which is consistent with the formation of larger particles [39, 46]. These observations further confirm the formation of larger particles [39, 46] when the MicroFactory incorporates the spherical agglomeration operation, thus suggesting that AE monitoring is a promising technique for studying spherical agglomeration.

Consistent with the previous continuous crystallisation experiment, samples were taken from the integrated process every 30 min (eight samples total). The resulting estimated PSD metrics are shown in Fig. 7b, and as minor variation was observed in the D_{10} and D_{50} measurements across the series, it can be concluded that a steady state was reached. The D90 does show an upward trend in 6 to 8 but remains within the standard deviation of the previous samples, until the final sample. A comparison of the estimated PSD from samples taken during the two continuous experiments confirms that the lovastatin particles increased in size during agglomeration. The average particle D_{50} size during the process increased from 139 to 247 µm ($\sigma = 27.1$). Comparative images of the suspension during particle size estimation qualitatively support the formation of lovastatin spherical agglomerates in the integrated MicroFactory (Fig. S6). The lovastatin spherical agglomerates contained bridges strong enough to survive the filtration, washing, and drying processes, and the measured PSD metrics of the isolated product are slightly larger than the estimated values from the process samples (Tables S4 and S5). The particle size D_{50} of the isolated agglomerates was 336 µm, more than double that of the product when the MicroFactory was operated using only a crystallisation operation (135 µm) and consistent with our process objective of 300 µm. A small number of primary particles remain within the isolated product, as indicated by a small shoulder in the overall distribution curve (Fig. 7c). but the vast majority of solid appears to be agglomerated with a larger particle size.

Particle Performance

A series of product characterisation and performance tests were performed on the resultant crystallised lovastatin and spherical agglomerate products. No significant differences were observed in the ToF–SIMS mass spectra acquired for the crystallised and spherically agglomerated lovastatin (Figs. S11 and S12). No additional species or potential contaminants were identified, and no BL was observed to be present in the spherically agglomerated lovastatin. The corresponding imaging data acquired for the two samples (Fig. 8) showed that the spherically agglomerated particles were larger than the crystallised particles, which is consistent with the PSD measurements.

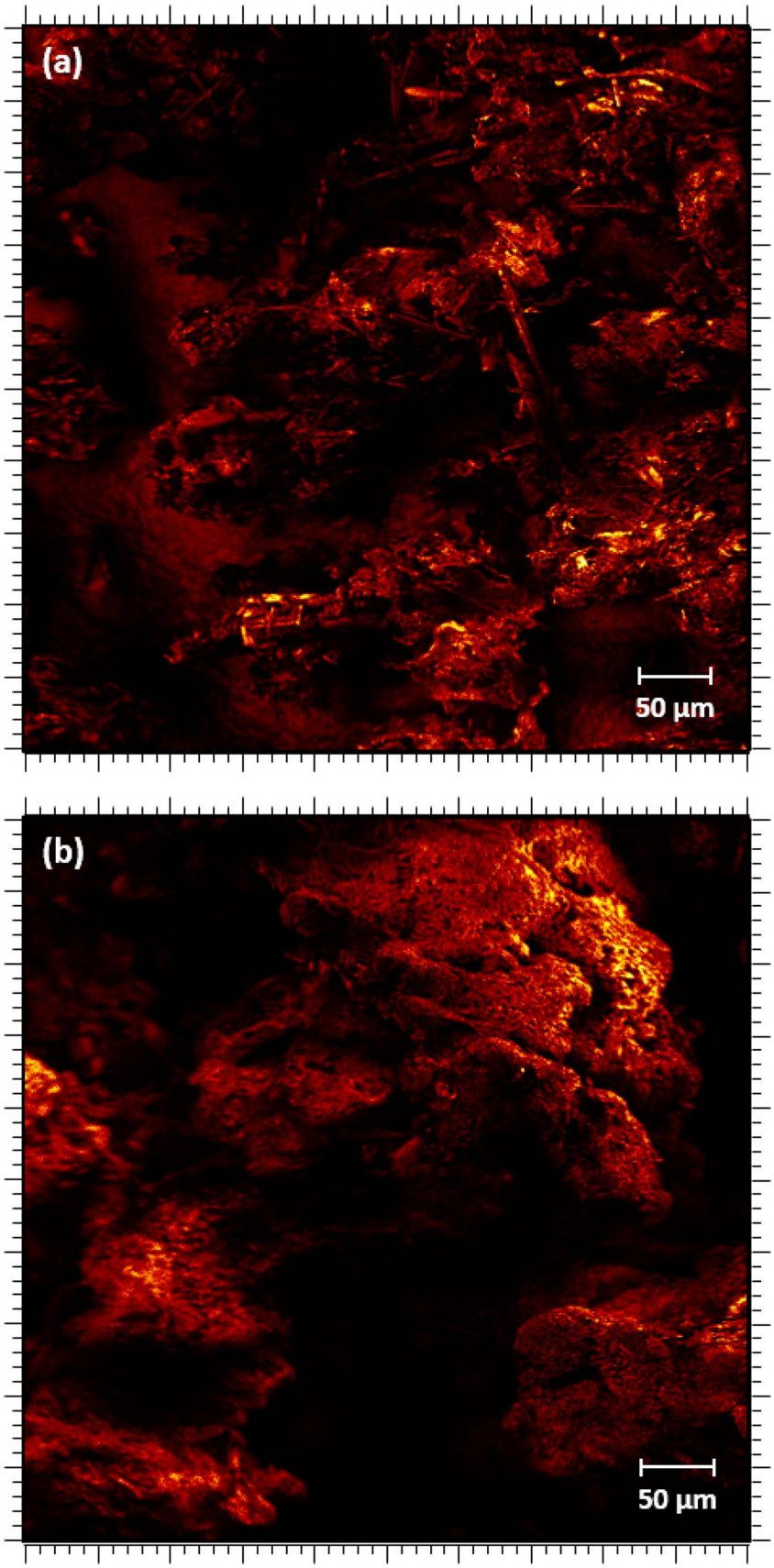

Fig. 8 ToF–SIMS image comparison between **a** crystallised lovastatin and **b** spherically agglomerated lovastatin. For clarity, both figures have been brightened in post-processing

Table 4 Comparison of pure crystallised and spherical agglomerated bulk particle properties

Particle	Tapped density (kg/m^3)	Bulk density (kg/m^3)	Hausner ratio	Median vol. wt. aspect ratio
Crystallised	591	428	1.38 (Poor)	0.69
Spherical agglomerate	541	461	1.17 (Good)	0.75

From the tapped and bulk density of the crystallised and spherically agglomerated powders, the Hauser ratio [47] was calculated as a measure of the powder's flowability (Table 4). The initial value of 1.38 for the non-agglomerated powder places it in the "poor" flow character [47]. Whereas the value of 1.17 for the spherical agglomerate powder characterises the powder as "good" confirming the improvement in this key manufacturability attribute [47]. The alteration of physical attributes due to spherical agglomeration was also reflected in the compactability of the various formulations (Fig. 7d). Most notably, it can be observed that for a fixed tensile strength, tablets produced from spherically agglomerated lovastatin have a significantly higher solid fraction, i.e. a less porous tablet. From the manufacturing classification system (MCS) [48] for oral solid dosage forms, properties of an ideal direct compression material would result in a compact with mechanical properties of a tensile strength > 1.0 MPa at ~ 0.85 solid fraction. Therefore, although tablets from compaction of neither pure lovastatin sample meet this specification at a tensile strength of > 1.0 MPa, tablets from crystallised lovastatin were more porous (solid fraction ~ 0.7 to 0.8) than those produced from spherically agglomerated lovastatin (solid fraction > 0.9). It was also observed that during tabletting, the crystallised lovastatin powder required external lubrication with sodium stearyl fumarate PG-100 to prevent the compacts laminating or becoming damaged during ejection. Whereas the spherically agglomerated lovastatin powder did not.

As lovastatin has a low therapeutic dose, 20/40/60 mg, to avoid the production of tablets with small physical dimensions blending with filler would be appropriate. In this case, comparison of tablet mechanical properties from formulations of 70:20:10 w% Pharmatose to Avicel to lovastatin with either crystallised or spherically agglomerated lovastatin at a dose of 20 mg showed a minor difference (Fig. 7d). This is due to the dilution of the influence of lovastatin on the mechanical properties, which will be dominated by Pharmatose and Avicel. In summary, spherical agglomeration of lovastatin has shown benefit in altering the bulk flow properties, compaction, and glidant performance of the pure materials without having any negative effects on the compaction properties of the formulated dosage form.

Discussion

A significant challenge when telescoping unit operations is the optimal inputs and outputs may not correlate across different processes, which was observed here when initially coupling the crystallisation, spherical agglomeration, and isolation of lovastatin. However, the compromises made are outweighed by the benefits of integrating operations. To avoid semibatch operation, the process throughput needed to be lowered, although the effect of this productivity decrease could be countered by the increase in lovastatin feed concentration. Furthermore, without modification of the solvent composition by dilution with water spherical agglomeration would not occur, as the MIBK added as BL would make a droplet-less single-phase solution, and this particle engineering process was key to improving the flowability and manufacturing properties of lovastatin in this MicroFactory. The increase in bulk density is highlighted when comparing 100% lovastatin tablets, where spherically agglomerated lovastatin resulted in less porous tablets. The improvements gained in powder processability by agglomerating the lovastatin crystals did not affect the compaction properties of tablets with a prescribable formulation.

Once completed, the physical footprint of the MicroFactory was 22.98 m^2. The product outlet after isolation in the crystallisation-spherical agglomeration mode produced 0.9 g of product material per minute, which subsequently required drying due to a mass fraction of n-heptane $X_{Hept} = 0.222$. Subject to the removal of this residual solvent residue, the fully integrated MicroFactory produced the equivalent of 11.6 doses of lovastatin 60 mg per minute, or 2800 doses during the 4-h process operating window.

Conclusions

A modular MicroFactory was developed for the integrated antisolvent crystallisation, spherical agglomeration, and isolation of lovastatin, successfully addressing the known challenges associated with its manufacture. Fouling of the PAT probes limited the quality of in situ data that could be generated. However, offline characterisation of the product showed that the flow properties of the needle-shaped crystals were improved by the addition of a spherical agglomeration operation, producing particles with a more favourable good (1.17)

Hausner ratio, which were suitable for direct compression. Using a single vessel for both particle engineering operations intensified the process and resulted in an overall footprint of 22.98 m^2 for the completed lovastatin MicroFactory.

When coupling and integrating batch processes for continuous operation, the flow rate into the crystalliser was reduced from 385.35 to 54.25 g/min, to ensure practical process volumes were used, and subsequently required changing the mixing strategy from X-mixer to CSTR. The feed concentration was increased from 0.0430 to 0.1784 g/g to accommodate the filtration platform requirements. The water content at the crystallisation end point was modified to facilitate spherical agglomeration through the addition of MIBK. The MicroFactory was operated in a crystallisation-only mode and crystallisation-spherical agglomeration mode, highlighting the system modularity achieved. Running all operations continuously can produce 696 doses of lovastatin per hour.

Abbreviations *AE*: Acoustic emission; *API*: Active pharmaceutical ingredient; *ATR*: Attenuated total reflectance; *AWL CFD25*: Alconbury Weston Ltd Continuous Filter Dryer 25; *BL*: Bridging liquid; *BSR*: Bridging liquid to solid ratio (mL/g); *CSTR*: Continuous stirred tank reactor; *DP*: Drug product; *ECV*: Equivalent cake volume (-); *EF*: Ejection force (kN); *FBRM*: Focused beam reflectance measurement; *FTIR*: Fourier transform infrared; *LPCF*: Lower punch compression force (kN); *LPD*: Lower punch displacement (mm); m_{API}: Mass of lovastatin primary particles (g); *MCS*: Manufacturing classification system; *MIBK*: Methyl isobutyl ketone; *NCE*: New chemical entity; *PC*: Principal component; *PCA*: Principal component analysis; *PLS*: Partial least squares; *rpm*: Rotations per minute; *SEM*: Scanning electron microscopy; *ToF-SIMS*: Time of flight secondary ion mass spectrometry; *UPCF*: Upper punch compression force (kN); *UPD*: Upper punch displacement (mm); V_{BL}: Volume of bridging liquid (mL); V_0: Unsettled apparent volume (bulk volume (kg/m^3)); V_{10}: Density after 10 taps (kg/m^3); V_{500}: Density after 500 taps (kg/m^3); V_{1250}: Density after 1250 taps (kg/m^3); σ: Standard deviation; τ: Residence time (min)

Supplementary Information The online version contains supplementary material available at https://doi.org/10.1007/s12247-024-09815-z.

Acknowledgements The authors thank Alconbury Western Ltd (AWL) for their technical support in modifying the AWL CFD25 filtration sequence operations and thank Syrris Ltd for the loan of a Dolomite Mitos P-Pump used during continuous crystallisation with spherical agglomeration experiments.

Author Contribution CJB: conceptualization, methodology, investigation, writing—original draft, review and editing, supervision. JMcG: methodology, investigation, writing—original draft. MTI: investigation. NR: investigation. OAT: investigation. SO: methodology, investigation, writing—original draft. MS: investigation. SJU: writing—original draft, review and editing. YSL: writing—original draft, review and editing. MWSC: investigation, writing—original draft. FP: investigation. ASP: investigation. EP: investigation. BS: investigation. JS: supervision, funding acquisition, writing—review and editing. JR: supervision, funding acquisition, writing—original draft. RS: supervision, funding acquisition. JDL: supervision, funding acquisition. CJP: supervision, funding acquisition. AN: supervision, funding acquisition, writing—review and editing. AJF: supervision, funding acquisition, writing —review and editing.

Funding Engineering and Physical Sciences Research Council, EP/P006965/1, Alastair James Florence, Higher Education Funding Council for England, HH13054,Alastair James Florence.

Availability of Data and Material All data underpinning this publication are openly available from the University of Strathclyde KnowledgeBase at https://doi.org/10.15129/bab0578c-f3b8-459a-8dc1-270a60f4c770.

Code Availability N/A.

Declarations

Ethics Approval N/A.

Consent to Participate N/A.

Consent for Publication N/A.

Conflict of Interest The authors declare no competing interests.

Open Access This article is licensed under a Creative Commons Attribution 4.0 International License, which permits use, sharing, adaptation, distribution and reproduction in any medium or format, as long as you give appropriate credit to the original author(s) and the source, provide a link to the Creative Commons licence, and indicate if changes were made. The images or other third party material in this article are included in the article's Creative Commons licence, unless indicated otherwise in a credit line to the material. If material is not included in the article's Creative Commons licence and your intended use is not permitted by statutory regulation or exceeds the permitted use, you will need to obtain permission directly from the copyright holder. To view a copy of this licence, visit http://creativecommons.org/licenses/by/4.0/.

References

1. Baxendale IR, Braatz RD, Hodnett BK, Jensen KF, Johnson MD, Sharratt P, et al. Achieving continuous manufacturing: technologies and approaches for synthesis, workup, and isolation of drug substance May 20–21, 2014 continuous manufacturing symposium. J Pharm Sci. 2015;104:781–91.
2. Lee SL, O'Connor TF, Yang X, Cruz CN, Chatterjee S, Madurawe RD, et al. Modernizing pharmaceutical manufacturing: from batch to continuous production. J Pharm Innov. 2015;10:191–9.
3. Burcham CL, Florence AJ, Johnson MD. Continuous manufacturing in pharmaceutical process development and manufacturing. Annu Rev Chem Biomol Eng. 2018;9:253–81.
4. Brown CJ, McGlone T, Yerdelen S, Srirambhatla V, Mabbott F, Gurung R, et al. Enabling precision manufacturing of active pharmaceutical ingredients: workflow for seeded cooling continuous crystallisations. Mol Syst Des Eng. 2018;3:518–49.
5. Ottoboni S, Price CJ, Steven C, Meehan E, Barton A, Firth P, et al. Development of a novel continuous filtration unit for pharmaceutical process development and manufacturing. J Pharm Sci. 2019;108:372–81.
6. Ottoboni S, Wareham B, Vassileiou A, Robertson M, Brown CJ, Johnston B, et al. A novel integrated workflow for isolation solvent selection using prediction and modeling. Org Process Res Dev. 2021;25:1143–59.
7. Moghtadernejad S, Escotet-Espinoza MS, Oka S, Singh R, Liu Z, Román-Ospino AD, et al. A training on: continuous manufacturing (direct compaction) of solid dose pharmaceutical products. J Pharm Innov. 2018;13:155–87.

8. Benyahia B, Lakerveld R, Barton PI. A plant-wide dynamic model of a continuous pharmaceutical process. Ind Eng Chem Res. 2012;51:15393–412.
9. Singh R, Muzzio F, Ierapetritou M, Ramachandran R. Plant-wide control of a continuous tablet manufacturing for quality-by-design based pharmaceutical manufacturing. Comput Aided Chem Eng. 2015;37:2183–8.
10. Domokos A, Nagy B, Gyürkés M, Farkas A, Tacsi K, Pataki H, et al. End-to-end continuous manufacturing of conventional compressed tablets: from flow synthesis to tableting through integrated crystallization and filtration. Int J Pharm. 2020;581.
11. Kirschneck D, Petek SM. End-to-end continuous manufacturing: chemical synthesis, workup and liquid formulation. Chim Oggi - Chem Today. 2017;35:28–30.
12. Mascia S, Heider PL, Zhang H, Lakerveld R, Benyahia B, Barton PI, et al. End-to-end continuous manufacturing of pharmaceuticals: integrated synthesis, purification, and final dosage formation. Angew Chem Int Ed. 2013;52:12359–63.
13. Testa CJ, Hu C, Shvedova K, Wu W, Sayin R, Casati F, et al. Design and commercialization of an end-to-end continuous pharmaceutical production process: a pilot plant case study. Org Process Res Dev. 2020;24:2874–89.
14. Badman C, Cooney CL, Florence AJ, Konstantinov K, Krumme M, Mascia S, et al. Why we need continuous pharmaceutical manufacturing and how to make it happen. J Pharm Sci. 2019;108:3521–3.
15. Bhalode P, Metta N, Chen Y, Ierapetritou M. Efficient data-based methodology for model enhancement and flowsheet analyses for continuous pharmaceutical manufacturing. Comput Aided Chem Eng. 2020;48:127–32.
16. Chen Y, Yang O, Sampat C, Bhalode P, Ramachandran R, Ierapetritou M. Digital twins in pharmaceutical and biopharmaceutical manufacturing: a literature review. Processes. 2020;8:1088.
17. Martin NL, Schomberg AK, Finke JH, Abraham TG, Kwade A, Herrmann C. Process modeling and simulation of tableting—an agent-based simulation methodology for direct compression. Pharmaceutics. 2021;13:996.
18. Spindler J, Kec T, Ley T. Lead-time and risk reduction assessment of a sterile drug product manufacturing line using simulation. Comput Chem Eng. 2021;152.
19. Urwin SJ, Chong MWS, Li W, McGinty J, Mehta B, Ottoboni S, et al. Digital process design to define and deliver pharmaceutical particle attributes. Chem Eng Res Des. 2023;196:726–49.
20. Chen D, Sirkar KK, Jin C, Singh D, Pfeffer R. Membrane-based technologies in the pharmaceutical industry and continuous production of polymer-coated crystals/particles. Curr Pharm Des. 2017;23:242–9.
21. Liu WJ, Ma CY, Wang XZ. Novel impinging jet and continuous crystallizer design for rapid reactive crystallization of pharmaceuticals. Procedia Engineering. 2015;102:499–507.
22. Raval V, Siddique H, Brown CJ, Florence AJ. Development and characterisation of a cascade of moving baffle oscillatory crystallisers (CMBOC). CrystEngComm. 2020;22:2288–96.
23. Zettl M, Aigner I, Mannschott T, van der Wel P, Schröttner H, Khinast J, et al. Characterization of a novel drying technology for continuous processing of cohesive materials: an ibuprofen case study. Org Process Res Dev. 2021;25:769–80.
24. Okazaki Y, Mishima N, Ashida K. Microfactory—concept, history, and developments. J Manuf Sci Eng. 2004;126:837–44.
25. Armstrong C, Miyai Y, Formosa A, Thomas D, Chen E, Hart T, et al. On-demand continuous manufacturing of ciprofloxacin in portable plug-and-play factories: development of a highly efficient synthesis for ciprofloxacin. Org Process Res Dev. 2021;25:1524–33.
26. Srai JS, Settanni E, Aulakh PK. Evaluating the business case for continuous manufacturing of pharmaceuticals: a supply network perspective. In: Nagy Z, El Hagrasy A, Litster J, editors. Continuous Pharmaceutical Processing. AAPS Advances in the Pharmaceutical Sciences Series, vol 42. Springer, Cham.
27. Rogers L, Jensen KF. Continuous manufacturing – the green chemistry promise? Green Chem. 2019;21:3481–98.
28. Capellades G, Neurohr C, Briggs N, Rapp K, Hammersmith G, Brancazio D, et al. On-demand continuous manufacturing of ciprofloxacin in portable plug-and-play factories: implementation and in situ control of downstream production. Org Process Res Dev. 2021;25:1534–46.
29. Lovette MA, Doherty MF. Needle-shaped crystals: causality and solvent selection guidance based on periodic bond chains. Cryst Growth Des. 2013;13:3341–52.
30. Hatcher LE, Li W, Payne P, Benyahia B, Rielly CD, Wilson CC. Tuning morphology in active pharmaceutical ingredients: controlling the crystal habit of lovastatin through solvent choice and non-size-matched polymer additives. Cryst Growth Des. 2020;20:5854–62.
31. McGinty J, Chong MWS, Manson A, Brown CJ, Nordon A, Sefcik J. Effect of process conditions on particle size and shape in continuous antisolvent crystallisation of lovastatin. Curr Comput-Aided Drug Des. 2020;10:925.
32. Kawashima Y, Cui F, Takeuchi H, Niwa T, Hino T, Kiuchi K. Improvements in flowability and compressibility of pharmaceutical crystals for direct tabletting by spherical crystallization with a two-solvent system. Powder Technol. 1994;78:151–7.
33. Pitt K, Peña R, Tew JD, Pal K, Smith R, Nagy ZK, et al. Particle design via spherical agglomeration: a critical review of controlling parameters, rate processes and modelling. Powder Technol. 2018;326:327–43.
34. Wang J, Li F, Lakerveld R. Process intensification for pharmaceutical crystallization. Chem Eng Process: Process Intensif. 2018;127:111–26.
35. Chen M, Liu X, Yu C, Yao M, Xu S, Tang W, et al. Strategy of selecting solvent systems for spherical agglomeration by the Lifshitz-van der Waals acid-base approach. Chem Eng Sci. 2020;220.
36. Ottoboni S, Coleman SJ, Steven C, Siddique M, Fraissinet M, Joannes M, et al. Understanding API static drying with hot gas flow: design and test of a drying rig prototype and drying modeling development. Org Process Res Dev. 2020;24:2505–20.
37. Allan P, Bellamy LJ, Nordon A, Littlejohn D. Non-invasive monitoring of the mixing of pharmaceutical powders by broadband acoustic emission. Analyst. 2010;135:518.
38. Nordon A, Waddell RJH, Bellamy LJ, Gachagan A, McNab D, Littlejohn D, et al. Monitoring of a heterogeneous reaction by acoustic emission. Analyst. 2004;129:463.
39. Nordon A, Carella Y, Gachagan A, Littlejohn D, Hayward G. Factors affecting broadband acoustic emission measurements of a heterogeneous reaction. Analyst. 2006;131:323–30.
40. Orehek J, Teslić D, Likozar B. Continuous crystallization processes in pharmaceutical manufacturing: a review. Org Process Res Dev. 2021;25:16–42.
41. Kougoulos E, Jones AG, Wood-Kaczmar MW. Estimation of crystallization kinetics for an organic fine chemical using a modified continuous cooling mixed suspension mixed product removal (MSMPR) crystallizer. J Cryst Growth. 2005;273:520–8.
42. European Medicines Agency. ICH guideline Q3C (R8) on impurities: guideline for residual solvents. 2021.
43. British Pharmacopoeia Commission. Appendix XVII: Bulk density and tapped density of powders. In: British Pharmacopoeia Commission. British Pharmacopoeia 2018: volume V: appendices. London: TSO.
44. Perciballi F. Formation of optimised particles for formulation and processing [Internet] [PhD Thesis]. University of Strathclyde; 2018. Available from: https://stax.strath.ac.uk/concern/theses/44558d285
45. Othmer DF, White RE, Trueger E. Liquid-liquid extraction data. Ind Eng Chem. 1941;33:1240–8.
46. Thorne PD, Foden DJ. Generation of underwater sound by colliding spheres. J Acoust Soc Am. 1988;84:2144–52.
47. United States Pharmacopeia and National Formulary. USP 114 powder flow. United States Pharmacopeial Convention [Internet].

2002; Available from: https://www.usp.org/sites/default/files/usp/document/harmonization/gen-chapter/g05_pf_30_6_2004.pdf
48. Leane M, Pitt K, Reynolds G. The manufacturing classification system (MCS) working group. A proposal for a drug product manufacturing classification system (MCS) for oral solid dosage forms. Pharm Dev Technol. 2015;20:12–21.

Publisher's Note Springer Nature remains neutral with regard to jurisdictional claims in published maps and institutional affiliations.